

## Research Paper

# Catalytic patch with redox Cr/CeO<sub>2</sub> nanozyme of noninvasive intervention for brain trauma

Shaofang Zhang<sup>1\*</sup>, Ying Liu<sup>1\*</sup>, Si Sun<sup>1\*</sup>, Junying Wang<sup>1</sup>, Qifeng Li<sup>4</sup>, Ruijuan Yan<sup>1</sup>, Yalong Gao<sup>4</sup>, Haile Liu<sup>1</sup>, Shuangjie Liu<sup>2</sup>, Wenting Hao<sup>2</sup>, Haitao Dai<sup>1</sup>, Changlong Liu<sup>1</sup>, Yuanming Sun<sup>3</sup>, Wei Long<sup>3</sup>✉, Xiaoyu Mu<sup>2</sup>✉, and Xiao-Dong Zhang<sup>1, 2</sup>✉

1. Tianjin Key Laboratory of Low Dimensional Materials Physics and Preparing Technology, Institute of Advanced Materials Physics, School of Sciences, Tianjin University, Tianjin, 300350, China.
2. Academy of Medical Engineering and Translational Medicine, Medical College, Tianjin University, Tianjin, 300072, China.
3. Tianjin Key Laboratory of Molecular Nuclear Medicine, Institute of Radiation Medicine, Chinese Academy of Medical Sciences and Peking Union Medical College, Tianjin, 300192, China.
4. Department of Neurosurgery and Key Laboratory of Post-trauma Neuro-repair and Regeneration in Central Nervous System, Tianjin Medical University General Hospital, Tianjin 300052, China.

\* These authors have contributed equally.

✉ Corresponding authors: Xiao-Dong Zhang (E-mail: xiaodongzhang@tju.edu.cn), Xiaoyu Mu (E-mail: muxiaoyu@tju.edu.cn) and Wei Long (E-mail: longway@irm-cams.ac.cn)

© The author(s). This is an open access article distributed under the terms of the Creative Commons Attribution License (<https://creativecommons.org/licenses/by/4.0/>). See <http://ivyspring.com/terms> for full terms and conditions.

Received: 2020.08.13; Accepted: 2020.12.07; Published: 2021.01.01

## Abstract

Traumatic brain injury (TBI) is a sudden injury to the brain, accompanied by the production of large amounts of reactive oxygen and nitrogen species (RONS) and acute neuroinflammation responses. Although traditional pharmacotherapy can effectively decrease the immune response of neuron cells via scavenging free radicals, it always involves in short reaction time as well as rigorous clinical trial. Therefore, a noninvasive topical treatment method that effectively eliminates free radicals still needs further investigation.

**Methods:** In this study, a type of catalytic patch based on nanozymes with the excellent multienzyme-like activity is designed for noninvasive treatment of TBI. The enzyme-like activity, free radical scavenging ability and therapeutic efficacy of the designed catalytic patch were assessed *in vitro* and *in vivo*. The structural composition was characterized by the X-ray diffraction, X-ray photoelectron spectroscopy and high-resolution transmission electron microscopy technology.

**Results:** Herein, the prepared Cr-doped CeO<sub>2</sub> (Cr/CeO<sub>2</sub>) nanozyme increases the reduced Ce<sup>3+</sup> states, resulting in its enzyme-like activity 3-5 times higher than undoped CeO<sub>2</sub>. Furthermore, Cr/CeO<sub>2</sub> nanozyme can improve the survival rate of LPS induced neuron cells via decreasing excessive RONS. The *in vivo* experiments show the Cr/CeO<sub>2</sub> nanozyme can promote wound healing and reduce neuroinflammation of mice following brain trauma. The catalytic patch based on nanozyme provides a noninvasive topical treatment route for TBI as well as other traumas diseases.

**Conclusions:** The catalytic patch based on nanozyme provides a noninvasive topical treatment route for TBI as well as other traumas diseases.

Key words: nanozyme, multienzyme-like activity, RONS-scavenging, traumatic brain injury, noninvasive treatment

## Introduction

Traumatic brain injury (TBI), one of the most common neurological diseases leading to disability and death, is caused by linear or rotational forces in the brain, producing large amounts of reactive oxygen

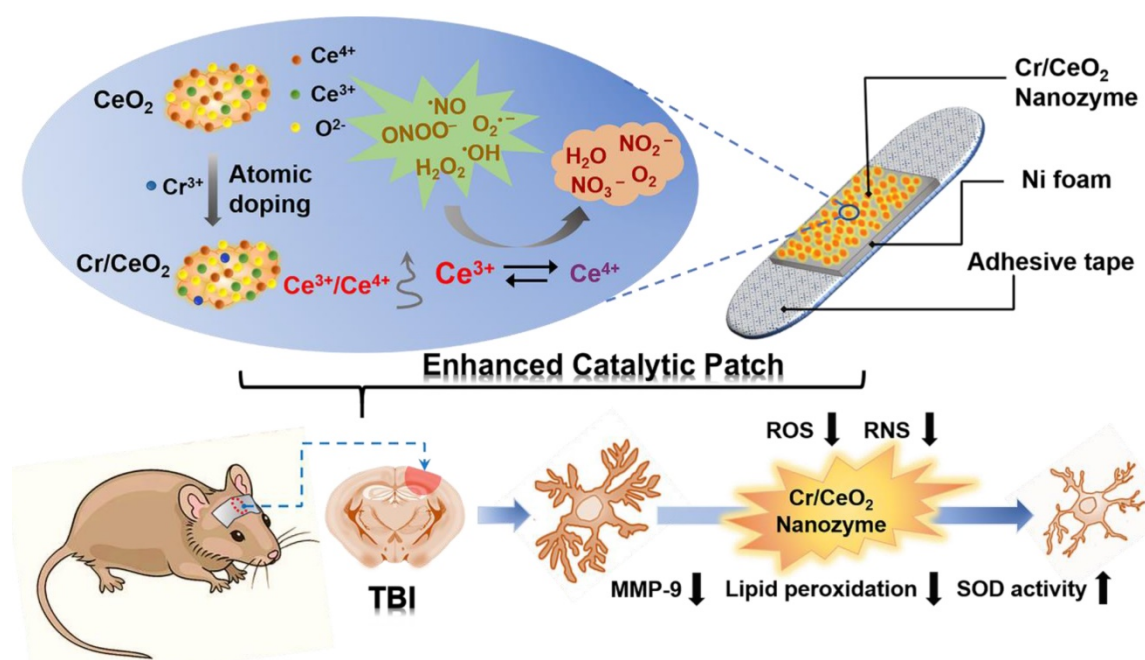
and nitrogen species (RONS) [1-4]. Subsequently, excessive free radicals diffuse into neuronal cells, and then oxidative stress induces inflammation of neuronal cells around the injured position [5-7].

Meanwhile, with increasing injury time, the secondary damage can further produce superoxide anion radicals ( $O_2^{\cdot-}$ ), hydroxyl radicals ( $\cdot OH$ ), peroxynitrite ( $ONOO^-$ ), hydrogen peroxide ( $H_2O_2$ ) and nitric oxide ( $\cdot NO$ ) in mitochondrion, which significantly aggravate oxidative damage and cause the continuous brain injury [8-12]. Therefore, the efficient clearance of RONS is crucial for the treatment of TBI [13-15].

At present, inorganic nanozymes, such as  $V_2O_5$ ,  $Fe_3O_4$ ,  $Mn_3O_4$  and  $CeO_2$ , have attracted widespread attentions due to their good controllability and enzyme-like activities [16-35], exhibiting a favorable prospect for the treatment of TBI. However, catalytic activity of nanozymes is suboptimal and the mimetic enzyme activities are singularized. For example, the  $V_2O_5$  nanozyme shows glutathione peroxidase (GPx)-like and peroxidase (POD)-like activity, displays poor performance in simulating superoxide dismutase (SOD) and catalase (CAT) [36-38]. The  $Fe_3O_4$  nanozyme also performs excellent POD-like activity, but low efficiency to SOD-like, CAT-like and GPx-like activities [39]. Similarly, it was reported that  $CeO_2$  nanozyme possesses enzyme mimetic properties, including SOD and CAT, due to its dual oxidation states can serve as an effective catalyst [40-41], but its GPx-like activity has rarely been mentioned before. Therefore, it is still necessary to further improve the catalytic activity of  $CeO_2$  with

multienzyme-like property for biomedical applications at ultralow treatment dose. Additionally, previous works have suggested that the ratio of  $Ce^{3+}/Ce^{4+}$  is one of the most important roles for catalytic efficiency, and the high ratio of  $Ce^{3+}/Ce^{4+}$  will induce the high catalytic activity due to increasing reduced state [42-44]. The Zirconia incorporated  $CeO_2$  induce a higher  $Ce^{3+}/Ce^{4+}$  ratio and faster conversion from  $Ce^{4+}$  to  $Ce^{3+}$  than those  $CeO_2$ , leading to significant improvement of RONS scavenging performance [45]. Thus, it is highly desirable to improve the catalytic property of  $CeO_2$  via doping engineering and develop the nanozyme patch for TBI treatment [46].

Herein, we developed a catalytic patch based on redox Cr-doped  $CeO_2$  ( $Cr/CeO_2$ ) nanozyme for noninvasive TBI treatment as shown in **Scheme 1**. The  $Cr/CeO_2$  nanozyme was synthesized by doping  $Cr^{3+}$  ions to improve the ratio of  $Ce^{3+}$  to  $Ce^{4+}$ , thereby improving the catalytic activity. The developed nanozyme displays multienzyme-like property, such as SOD, CAT and GPx, and scavenging activity to free radicals, including  $\cdot OH$ ,  $ONOO^-$  and  $H_2O_2$ , which are remarkably higher than that of undoped  $CeO_2$ . Furthermore, the nanozyme patch can diminish the accumulation of RONS in injured cells, and be helpful for improving wound healing of TBI via reducing the neuroinflammation.



**Scheme 1.** Noninvasive intervention mechanism for brain trauma via enhanced catalytic patch with redox  $Cr/CeO_2$  nanozyme.

## Methods

### Materials

Cerium(III) nitrate hexahydrate ( $\text{Ce}(\text{NO}_3)_3 \cdot 6\text{H}_2\text{O}$ , 99.5% metal basis) and Chromic nitrate nonahydrate ( $\text{Cr}(\text{NO}_3)_3 \cdot 9\text{H}_2\text{O}$ , 99%) were purchased from Shanghai Macklin Biochemical Co., Ltd. (China). ethylenediaminetetraacetic (EDTA, 99.5%) and citric acid were obtained by Shanghai Aladdin Biochemical Co., Ltd. (China). Ammonium hydroxide ( $\text{NH}_3 \cdot \text{H}_2\text{O}$ , 30% basis) and ethanol were purchased from Jiangtian chemical industry (China). Horseradish peroxidase (HRP) was purchased from Sigma-Aldrich, which was of 300 IU/mg of lyophilized solid. All aqueous solutions in the experiment were using deionized water (Millipore, 18.2 M $\Omega$  cm). All compounds used are analytically pure.

### Synthesis of Cr-doped ceria nanozyme ( $\text{Cr}/\text{CeO}_2$ )

In the work, the monodisperse  $\text{Cr}/\text{CeO}_2$  nanozyme with an elliptical shape was prepared by coprecipitation method. Initially, to a 30 mL beaker was added citric acid (0.048 g) and EDTA (0.073 g), followed by deionized water (10 mL). Place the beaker under a high-speed magnetic stirring at 1000 rpm in air. Meanwhile,  $\text{Cr}(\text{NO}_3)_3 \cdot 9\text{H}_2\text{O}$  (0.8 g) was dissolved in deionized water (2 mL) to form the aqueous solution of  $\text{Cr}(\text{NO}_3)_3$  (1 mmol/mL). Then  $\text{Ce}(\text{NO}_3)_3 \cdot 6\text{H}_2\text{O}$  (0.7814 g) and  $\text{Cr}(\text{NO}_3)_3$  aqueous solution (200  $\mu\text{L}$ ) was added to the beaker. The clear solution turned a dark blue in color. Subsequently, 28%-30% ammonium hydroxide (260  $\mu\text{L}$ ) was added under vigorous stirring. The solution was stirred for 2 h at room temperature to form a cloudy solid-liquid mixture. Then, the precipitate in the mixture was collected by centrifugation for 5 min and washed several times with distilled water and ethanol, respectively, to remove the unreacted reactants and impurities. Afterwards, dried at 120 °C for 12 h in oven. Eventually, the obtained dark blue powder was calcined at 550 °C for 4 h to form dark brown powder, namely  $\text{Cr}/\text{CeO}_2$ . In addition,  $\text{Cr}(\text{NO}_3)_3 \cdot 9\text{H}_2\text{O}$  was replaced by  $\text{AgNO}_3$ ,  $\text{Co}(\text{NO}_3)_2 \cdot 6\text{H}_2\text{O}$ ,  $\text{RhCl}_3 \cdot 3\text{H}_2\text{O}$ ,  $\text{Mn}(\text{NO}_3)_2 \cdot 4\text{H}_2\text{O}$ ,  $\text{PdCl}_2$  or  $\text{Ni}(\text{NO}_3)_2 \cdot 6\text{H}_2\text{O}$  to synthesize  $\text{CeO}_2$  nanozymes doped with different metal elements, which were named by  $\text{M}/\text{CeO}_2$ . The prepared  $\text{M}/\text{CeO}_2$  nanozymes were used in the following characterization and biomedical applications.

### Preparation of catalytic patch with $\text{Cr}/\text{CeO}_2$ nanozyme

First, the porous nickel foams were treated with

dilute hydrochloric acid, acetone, ethanol, and deionized water for 10 min, respectively. Then, the purified  $\text{Cr}/\text{CeO}_2$  nanozyme were dispersed in water by ultrasound. The nickel foams were soaked in the solution containing nanoparticles in a 120 °C oven for 12 h. Finally, the nickel foams loaded with nanoparticles were annealed at 550 °C for 4 h. The catalytic patch was affixed to a viscous material for later use.

### Characterization

TEM and X-ray spectroscopy (EDX) elemental mapping images of as-prepared  $\text{Cr}/\text{CeO}_2$  nanozyme sample were taken on a JEOL-2000EX transmission electron micrograph, with accelerating voltage of 200 kV. X-ray diffraction technology was used to investigate the crystal structure of XRD spectra were conducted on X-ray Powder diffractometer (D/MAX-2500, Rigaku, Japan) with  $\text{Cu K}\alpha$  radiation. The valence states of elements measured by X-ray photoelectron spectrometer (PHI 1600, Perkin Elmer, USA) with the  $\text{Al K}\alpha$  excitation. Optical properties were measured characterized by ultraviolet-visible (UV-vis) absorption spectroscopy operating at a Varian Lambda 750 UV-VIS NIR instrument (Shimadzu, Japan) while the cuvette was utilized to contain  $\text{Cr}/\text{CeO}_2$  nanozyme hydration solutions.

### Multienzyme-like activity evaluation

This experiments were carried out by a modified procedure according to previous reports [47]. The 3,3',5',5'-tetraMethyl benzidine (TMB) substrate color development kit (ELISA) was used to detect the POD-like activity of  $\text{Cr}/\text{CeO}_2$  nanozyme. According to the instructions, TMB buffer, TMB color developing solution and TMB oxidizing agent are mixed at a ratio of 5000:5000:4 to prepare the TMB color developing working solution. The TMB buffer consists of an acetate buffer with a pH of 6. In 96-well plates, the  $\text{Cr}/\text{CeO}_2$  nanoenzyme (20  $\mu\text{L}$ ) with different concentrations (0.1, 0.4, 0.8, 1.5, 3 and 6 mg/mL) were added, followed by TMB color developing working solution (200  $\mu\text{L}$ ) and incubated for 30 min at room temperature in the dark. At the same time, the evolution of absorbance at 630 nm with time was measured though a microplate spectrophotometer (CMax Plus, Molecular Devices). Eventually, the reaction solution turned blue and photographed for recording. In addition,  $\text{Cr}/\text{CeO}_2$  nanoenzyme replaced by deionized water (20  $\mu\text{L}$ ) was used as blank control.

The SOD-like activity of  $\text{CeO}_2$  and  $\text{Cr}/\text{CeO}_2$  nanozyme were studied by classical nitro-blue tetrazolium (NBT) chromogenic method. According to experimental scheme, a SOD working solution

were prepared by mixing SOD detection buffer (250  $\mu\text{L}$ ), NBT color developing solution (75  $\mu\text{L}$ ) and NBT enzyme solution (75  $\mu\text{L}$ ). Then,  $\text{CeO}_2$  (3 mg/mL, 50  $\mu\text{L}$ ) or Cr/ $\text{CeO}_2$  (3 mg/mL, 50  $\mu\text{L}$ ) nanozymes were added to the SOD working solution (400  $\mu\text{L}$ ), respectively. Subsequently, the reaction start solution (50  $\mu\text{L}$ ) was added and illuminated for 10 min. The absorbance of formazan at 560nm with reaction time was detected by UV-vis spectrophotometer, indicating the superoxide scavenging ability. In addition, the difference in absorbance of reduced formazan was collected by varying the concentration of Cr/ $\text{CeO}_2$  nanozyme (0-6 mg/mL). Finally, the SOD-like activity of the nanozyme, the clearance rate of superoxide and the concentration-dependent SOD-like activity were calculated by colorimetric analysis.

The CAT-like activity of  $\text{CeO}_2$  and Cr/ $\text{CeO}_2$  nanozymes were evaluated by measuring the decrease in absorbance of  $\text{H}_2\text{O}_2$  at 240 nm. First, the absorption spectrum of  $\text{H}_2\text{O}_2$  solution (50  $\mu\text{mol/L}$ ) is measured by UV-vis spectrophotometer. Then,  $\text{CeO}_2$  (3 mg/mL, 10  $\mu\text{L}$ ) or Cr/ $\text{CeO}_2$  nanozymes (3 mg/mL, 10  $\mu\text{L}$ ) were mixed with  $\text{H}_2\text{O}_2$  solution (50  $\mu\text{mol/L}$ , 190  $\mu\text{L}$ ) and incubated for 2 h in the dark. Then, the mixed solutions with generated bubbles were photographed and the absorption spectra were obtained, respectively. Finally, the clearance rate of  $\text{H}_2\text{O}_2$  was quantified.

The GPx-like activity of Cr/ $\text{CeO}_2$  nanozyme was determined adopting the classical Glutathione reductase (GR)-coupled assay by detecting the decrease in absorbance of reduced nicotinamide adenine dinucleotide phosphate (NADPH) at 340 nm. In a assay, the reaction solution is mixed by Cr/ $\text{CeO}_2$  nanozyme (3 mg/mL, 30  $\mu\text{L}$ ), reduced glutathione (GSH) (2 mmol/L, 50  $\mu\text{L}$ ), GR (17 units, 50  $\mu\text{L}$ ), NADPH (200  $\mu\text{mol/L}$ , 50  $\mu\text{L}$ ),  $\text{H}_2\text{O}_2$  (1 mmol/L, 10  $\mu\text{L}$ ) and pH 7.4 phosphate buffer (310  $\mu\text{L}$ ). Then, the reaction was monitored during 10 min on a UV-vis spectrophotometer operating under kinetic mode. Next, the concentrations-dependent GPx-like activity of Cr/ $\text{CeO}_2$  nanozyme was tested by varying the doses of Cr/ $\text{CeO}_2$  nanozyme (0-70  $\mu\text{L}$ ), while other reactants are fixed. The GPx-like activity of  $\text{CeO}_2$  enzyme was used as a control in the experiment. Finally, the corresponding reaction rate was calculated.

### Kinetic analysis

Steady-kinetic measurements were conducted by monitoring the absorbance change at 652 nm on a microplate reader [48]. The assay was performed using 50  $\mu\text{g/mL}$  Cr/ $\text{CeO}_2$  nanozyme or 0.02 ng/mL HRP in a reaction volume of 200  $\mu\text{L}$  sodium acetate

buffer solution (pH 4) with 800  $\mu\text{M}$  TMB and 50 mM  $\text{H}_2\text{O}_2$  as substrates. When the 800  $\mu\text{M}$  TMB as substrate is fixed, the concentration of  $\text{H}_2\text{O}_2$  is varied: 0, 0.025, 0.25, 0.5, 1, 2.5, 5, 25 and 50 mM. On the contrary, the 50 mM  $\text{H}_2\text{O}_2$  as substrate is fixed, the concentration of TMB is varied: 0, 12.5, 25, 50, 100, 200, 400 and 800  $\mu\text{M}$ . Then, maximum initial velocity ( $V_{max}$ ) and Michaelis-Menten constant ( $K_m$ ) were calculated using Lineweaver-Burk plots of the double reciprocal of the Michaelis-Menten equation,  $1/v = K_m/V_{max} \cdot (1/[S] + 1/K_m)$ , where  $v$  is the initial velocity and  $[S]$  is the concentration of substrate.

### RONS scavenging capacities of Cr/ $\text{CeO}_2$ nanozyme

The  $\cdot\text{OH}$  scavenging capacity of Cr/ $\text{CeO}_2$  nanozyme was qualitatively tested by electron spin resonance (ESR) spectroscopy (Bruker EMX plus, Germany). In the experiment, 5-tert-Butoxycarbonyl-5-methyl-1-pyrroline N-oxide (BMPO) (1 mg) was dissolved in buffer (195  $\mu\text{L}$ , potential of hydrogen: 7.2-7.4) and  $\text{H}_2\text{O}_2$  (5  $\mu\text{L}$ , 40 mmol/L) was added. The mixture was irradiated under a UV lamp for 5 min to generate  $\cdot\text{OH}$ , of which BMPO was a capture agent. Then, comparing the intensity of the ESR spectrum with or without the presence of  $\text{CeO}_2$  or Cr/ $\text{CeO}_2$  nanozyme (6 mg/mL, 10  $\mu\text{L}$ ).

The  $\text{O}_2^{\cdot-}$  scavenging capacity is recorded by ESR spectroscopy as described above.  $\text{O}_2^{\cdot-}$  is derived from  $\text{KO}_2$  with ultraviolet light treatment and accurately tapped by BMPO. The specific operation was as follows: 18-crown-6 (1 mg) was dissolved in a medium solution of DMSO (10.81 mL) to form an 18-crown-6 solution (3.5 mmol/L), which was stored in a refrigerator.  $\text{KO}_2$  (2 mg) is fully dissolved in the 18-crown-6 solution (562.5  $\mu\text{L}$ , 3.5 mmol/L) under ultrasound, followed by the addition of BMPO (25 mmol/L). Subsequently, the mixture was exposed to UV light for 5 min to produce  $\text{O}_2^{\cdot-}$ , and ESR spectra were collected as a blank control in time. The ESR spectra were again measured and analyzed after adding  $\text{CeO}_2$  or Cr/ $\text{CeO}_2$  nanozymes (6 mg/mL, 10  $\mu\text{L}$ ), respectively.

$\cdot\text{NO}$  radicals are obtained by a combination of Carboxy-PTIO and S-nitroso-N-acetyl-penicillamine (SNAP), while EPR spectra, as above-mentioned, are applied to assess the  $\cdot\text{NO}$  scavenging ability. In a typical trial, the first step is to dilute the Carboxy-PTIO (250 mmol/L) to 10  $\mu\text{mol/L}$  with phosphate-buffered saline (PBS) and disperse SNAP (1 mg) in PBS (900  $\mu\text{L}$ ) to acquire SNAP solution (5 mmol/L). Thereafter, the final solution consisted of the Carboxy-PTIO solution (190  $\mu\text{L}$ , 10 mmol/L) and the SNAP solution (10  $\mu\text{L}$ , 5 mmol/L), and the reaction was carried out for 15 min to engender  $\cdot\text{NO}$ .

The 7-peak signals were examined through the ESR spectra. Eventually, add CeO<sub>2</sub> or Cr/CeO<sub>2</sub> nanozymes (6 mg/mL, 10 µL) to measure again and appraise the difference in ESR spectra was with and without nanozymes.

Due to ONOO<sup>-</sup> has a significant absorption peak at 302 nm, the ONOO<sup>-</sup> scavenging ability was represented by detecting the change of the absorption spectrum in the range of 200-600 nm on a UV-vis spectrophotometer. First, HCl (1 mol/L), NaOH (1.5 mol/L), NaNO<sub>2</sub> (50 mmol/L), and H<sub>2</sub>O<sub>2</sub> (25 mmol/L) aqueous solutions were prepared. Then, 10 mL of NaNO<sub>2</sub> solution and 10 mL of H<sub>2</sub>O<sub>2</sub> were blended and stirred for 3 min, followed by 5 mL of HCl solution and rapidly injected 5 mL of NaOH solution. It is especially critical that the entire formulation process is carried out in an ice bath. As a result, the solution turned pale yellow to indicate the production of the ONOO<sup>-</sup>. Afterwards, UV-vis spectrophotometer is selected to quantitatively dilute the concentration of ONOO<sup>-</sup>, i.e., the absorbance at 302 nm (A<sub>302</sub>) is about 0.7. Thereafter, CeO<sub>2</sub> or Cr/CeO<sub>2</sub> nanozymes (3 mg/mL, 10 µL) were added to the weak solution (190 µL) to observe the decrease of A<sub>302</sub> with the reaction time, and the reduction in ONOO<sup>-</sup> itself was measured as the background value in the same time. Finally, the actual value of ONOO<sup>-</sup> elimination under the action of nanozymes was calculated by deducting the background value.

For 1,1-diphenyl-2-picrylhydrazyl (DPPH) scavenging capacity, the absorption spectrum was selected to record at 300-700 nm due to its characteristic peak at 535 nm. In a typical assay, DPPH is dissolved in DMSO as a stock solution and then diluted to 25 µmol/L with deionized water with an absorbance at 535 nm (A<sub>535</sub>) of approximately 0.42. The A<sub>535</sub> was measured by the addition of DPPH solution (195 µL) in the cuvette, and the absorption spectrum was measured after adding CeO<sub>2</sub> or Cr/CeO<sub>2</sub> nanozymes (6 mg/mL, 5 µL) at intervals of 10 min. The time dependence of the diminishable on A<sub>535</sub> was evaluated with the addition of nanozyme, which is the DPPH scavenging capacity of the nanozyme.

### Cell toxicity

In a 96-well plate, HT22 cells were cultured with Dulbecco's modified eagle medium (DMEM) at 37 °C (about 4000 cells per well). After 12 h of growth, a series of CeO<sub>2</sub> or Cr/CeO<sub>2</sub> nanozyme solutions were added into each well at a dose of 6 to 100 µg/mL, respectively. The cells were then incubated for another 24 h and the cell viabilities were measured by MTT assay.

### Cell survival

HT22 cells were seeded in 96-well plates (approximately 2000 per well) and grown for 12 h in a 37-read incubator. A series of CeO<sub>2</sub> or Cr/CeO<sub>2</sub> nanozyme solutions at a dose of 6 to 100 µg/mL were added into wells and maintained for 24 h to promote cell uptake. Then, the cells were incubated for another 24 h under stimulation with lipopolysaccharide (LPS) solutions (0.5 mg/mL, respectively). Finally, the corresponding cell viabilities were quantified by MTT assay.

### In vitro free radical detection

HT22 cells were seeded into 6-well plates at 15,000 cells per well and cultured until fully adherent. First, the DMEM containing CeO<sub>2</sub> nanozyme (25 µg/mL) or Cr/CeO<sub>2</sub> nanozyme (25 µg/mL) was added into each well, followed by LPS (0.5 mg/mL). After 6 h of incubation, DCFH-DA ((S0033S, Beyotime), DHE (S0063, Beyotime) or DAF-FM DA (S0019, Beyotime) reagents were added into the 6-well culture plates to detect cellular total ROS, O<sub>2</sub><sup>•-</sup> and •NO levels. After a period of time (DCFH-DA, DHE and DAF-FM DA correspond to reaction times of 20, 30 and 20 min, respectively), the plate was washed three times with PBS to stop the reaction. The CeO<sub>2</sub> nanozyme was used as a control in the experiment. Finally, cell images were captured using a fluorescence microscope (EVOS, AMG) and quantitative analysis was performed by flow cytometry (BD Accuri™ C6). The difference in fluorescence intensity was compared to analyze the level of free radicals in cells.

### Traumatic brain injury (TBI)

C57 BL/6 male mice at 8-10 weeks age with a body weight of 21-23 g were selected to establish TBI model with fluid percussion injury. Each mouse was anesthetized by intraperitoneal injection of 0.2 µL of 10% chloral hydrate. After anesthesia, the head of the mouse was depilated and the skin was cut to separate the meninges from the skull. Then, the head of the mouse was fixed on a stereo azimuth instrument, and a nearly circular opening having a diameter of 5 mm in the right brain was cut with a dental drill. Next, a craniocerebral instrument was used to hit the round hole in the right brain of mouse. During all animal experiments, the specific trauma was made by opening the bone window with a fluid percussion injury (1.7 ± 0.1 atm) for moderate TBI models. Subsequently, the brain injured mice were randomly divided into three groups: TBI mice without treatment (TBI), TBI mice with CeO<sub>2</sub> nanozyme patch treatment (TBI+CeO<sub>2</sub>), TBI mice with Cr/CeO<sub>2</sub> nanozyme patch treatment (TBI+Cr/CeO<sub>2</sub>), photographs of the wound

were taken once every two days. Finally, a catalytic patch loaded with CeO<sub>2</sub> or Cr/CeO<sub>2</sub> nanozymes was adhered to the brain of mice in TBI+CeO<sub>2</sub> or TBI+Cr/CeO<sub>2</sub> groups and replaced every other day.

In addition, we further investigated the concentration and diffusion depth of Cr/CeO<sub>2</sub> nanozyme released from the patch into brain tissue. Taking the injury location as the starting point, brain slices were made each 2 mm along the longitudinal direction, and then the concentration of Cr/CeO<sub>2</sub> nanozyme in each section was measured by the inductively coupled plasma mass spectroscopy (ICP-MS).

### Immunofluorescence

Mice in the normal control, TBI, TBI+CeO<sub>2</sub>, and TBI+Cr/CeO<sub>2</sub> groups were perfused, and the brains were removed and fixed in 4% paraformaldehyde. Then, the brain tissue was made into paraffin slices. The slices were stained by the following procedures: dewaxing in xylene, dehydration in gradient ethanol (100%, 95%, 80%, and 70%), antigen retrieval in sodium citrate or EDTA solutions, addition of primary antibody overnight at 4 °C, incubation with goat anti rabbit IgG 488 or 594 secondary antibody for 1 h, staining of nuclei with DAPI for 5 min and sealing with fluorescence quencher. For primary antibody, anti-GFAP, Iba1 and matrix metalloproteinase-9 (MMP-9) (Proteintech) were used to stain astrocytes, microglia and MMP-9, respectively. Notably, the staining process was carried out in the dark. Finally, the stained images were acquired by fluorescence microscope (EVOS, AMG) and immunofluorescence analysis was performed by Image J software.

### In vivo oxidative stress

Mice were perfused with normal saline on 12 and 26 days after TBI and brains were taken. SOD activity was evaluated according to the experimental protocol in the Total Superoxide Dismutase Assay Kit with WST-8 (Beyotime, S0101). Brain tissue and SOD sample preparation solution were added into centrifuge tube at a mass ratio of 1:10, and homogenized in ice bath. The brain homogenate was centrifuged and the supernatant was used as a sample to be tested. Meanwhile, the SOD standard was diluted to the following series concentrations: 1, 2, 5, 10, 20, 50 and 100 U/mL, for making a standard curve. Then, WST-8 enzyme working solution (160 μL), sample (20 μL) and reaction start solution (20 μL) were sequentially added to the 96-well plate for 30 min, and the absorbance at 450 nm was detected by a multifunctional microplate detector (Synergy HT). The SOD activity of brain tissue was calculated with reference to the standard curve.

The lipid peroxide assay was performed using the Lipid Peroxidation malondialdehyde (MDA) assay kit (Beyotime, S0131). According to the instructions, the brain tissue was homogenized in PBS. At the same time, the standard was diluted to 1, 2, 5, 10, 20 and 50 μmol/L with distilled water to prepare a standard curve. Then, the sample (100 μL) was mixed with MDA test working solution (200 μL) and heated in boiling water for 15 min. The absorbance at 532 nm was measured with a multifunctional microplate detector (Synergy HT). Further, the protein concentration of the sample was measured using BCA Protein Assay Kit (Beyotime, P0010). Finally, the MDA content per unit weight of protein in brain tissue was quantified by the standard curve.

### Morris water maze test

The Morris water maze test was used to assess the differences of spatial learning ability and related memory in the four groups of mice (control, TBI, TBI+CeO<sub>2</sub>, and TBI+Cr/CeO<sub>2</sub>). First, a Morris water maze model was built by injecting 50 cm of water into a large cylindrical water tank, than adding non-toxic white paint to make the water opaque. The water tank is divided into four quadrants, and the platform is hidden about 1 cm below the water surface in the middle of the quadrant I. Video tracking of mice was performed using a camera focused on the tank. The hidden platform training period lasted for 5 days and 4 trials were conducted each day, with the starting sites being located at fixed positions in four different quadrants of the tank wall. In the trial, the mouse found the platform and ended the timing when it was held on the platform for 2 seconds. The maximum duration of the training was 60 seconds. Mice that failed to reach the platform within 60 seconds were directed to the platform and held for 10 seconds. The time to reach the platform, the distance from the platform, and the average swimming speed were recorded during the five days. On the fifth day, the platform was removed and each mouse was allowed to swim for 60 seconds. The spatial learning ability and related memory ability of the mice were evaluated by recording the frequency of the mice through the platform, the average distance to the platform, and the time spent in the first quadrant.

### Hematological test

Mice in TBI, TBI+CeO<sub>2</sub> and TBI+Cr/CeO<sub>2</sub> groups were subjected to ocular blood extraction at 12 and 26 days after TBI. The hematological examination of blood was performed in time. Then, the serum was collected by centrifuging for biochemical analysis.

## Statistical analysis

All data in this work were presented as mean  $\pm$  standard deviation (SD). The statistical analysis was executed by a Student's *t* test.

## Result and Discussion

### Characterization of Cr/CeO<sub>2</sub> nanozyme

The Cr/CeO<sub>2</sub> nanozymes were synthesized by the method of coprecipitation [40, 49]. X-ray diffraction (XRD) technology was used to investigate the crystal structure of Cr/CeO<sub>2</sub>. As shown in **Figure 1A**, the (111) and (200) diffraction peaks can be found in both CeO<sub>2</sub> and Cr/CeO<sub>2</sub>, identifying high crystallinity. Meanwhile, the diffraction angles corresponding to (111) and (200) show the significant shift to a large angle after Cr doping, indicating that the incorporation of Cr<sup>3+</sup> ions with small atomic radius into CeO<sub>2</sub> induces lattice distortion. Meanwhile, the UV-vis absorption spectrum in **Figure 1B** shows that a slight red shift in the absorption band edge after Cr doping, suggesting decrease of band gap.

In order to further elucidate detailedly the structural composition, the X-ray photoelectron spectroscopy (XPS) tests of Cr/CeO<sub>2</sub> and pure CeO<sub>2</sub> were performed. As shown in **Figure 1C-D**, the Ce possesses the dual oxidation state of the +3 and +4 valence states, and Ce<sup>4+</sup> is located at 907.3, 900.8, 916.6 eV and 889, 898.3, 882.5 eV, ascribed to Ce<sup>4+</sup> 3d<sub>3/2</sub> and Ce<sup>4+</sup> 3d<sub>5/2</sub>, respectively. The peaks at 885.3 and 903.8 eV are assigned to Ce<sup>3+</sup> 3d<sub>3/2</sub> and Ce<sup>3+</sup> 3d<sub>5/2</sub>. In addition, the two peaks at 587 and 577.3 eV in **Figure 1E** correspond to the binding energies of Cr<sup>3+</sup> 2p<sub>1/2</sub> and Cr<sup>3+</sup> 2p<sub>3/2</sub>, revealing the presence of Cr<sup>3+</sup> ions. Quantative analysis in **Figure 1F** reveals Cr<sup>3+</sup> incorporation promotes an increase in the ratio of Ce<sup>3+</sup> to Ce<sup>4+</sup>, as well as production of reduced Cr<sup>3+</sup> state. Furthermore, the transmission electron microscopy (TEM) and high-resolution TEM (HRTEM) images of Cr/CeO<sub>2</sub> nanozyme in **Figure S1** and **1G** reveal that the size of nanozyme is about 8~12 nm, and interplanar spacing of the (111) plane of CeO<sub>2</sub> is slightly reduced from 0.3123 Å to ~0.3047 Å after Cr doping. Additionally, the energy dispersive X-ray spectroscopy (EDX) mapping of Cr/CeO<sub>2</sub> nanozyme in **Figure 1H** also indicates Cr doping into CeO<sub>2</sub>.

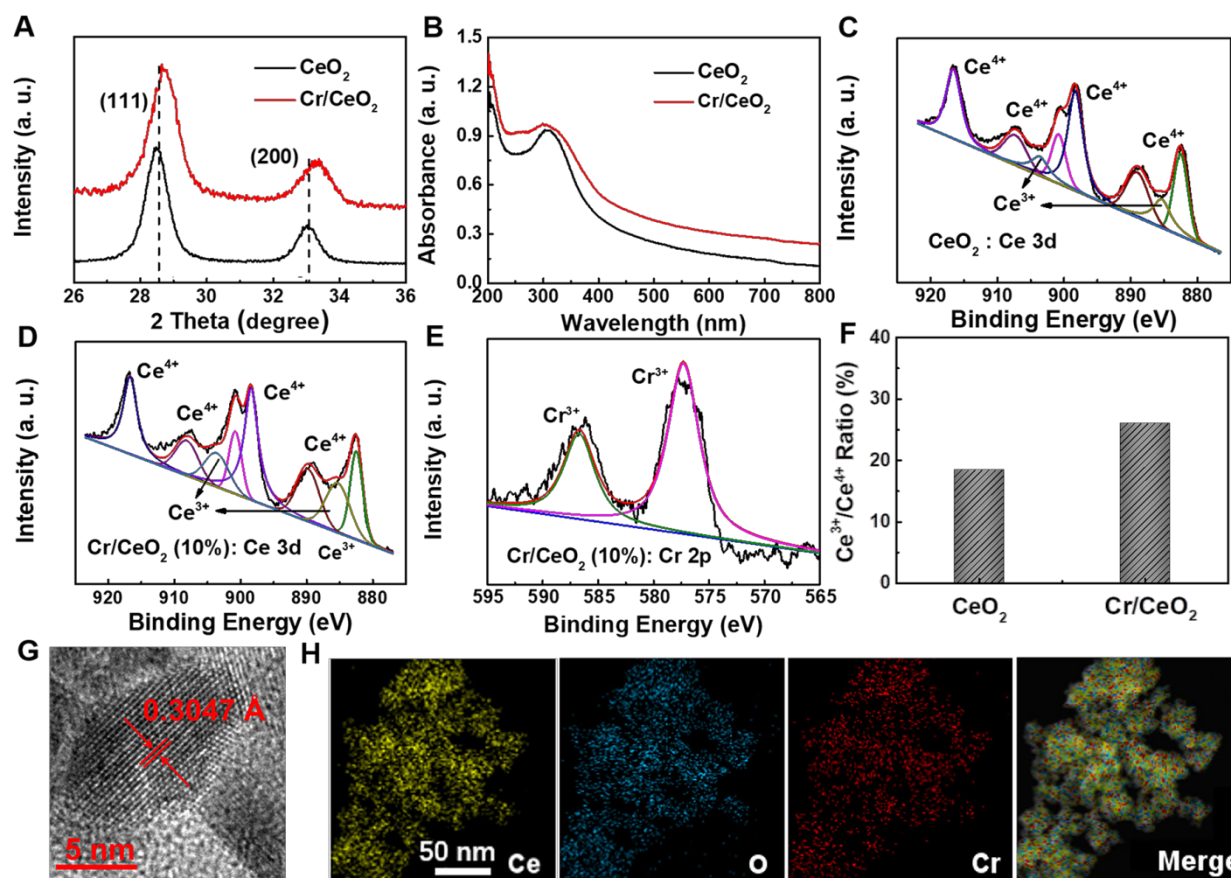


**Figure 1. Materials Properties of Cr/CeO<sub>2</sub> nanozyme.** **A)** XRD pattern of CeO<sub>2</sub> and Cr/CeO<sub>2</sub> nanozymes. **B)** UV-vis absorption spectra of CeO<sub>2</sub> and Cr/CeO<sub>2</sub> nanozymes. **C)** XPS spectra of CeO<sub>2</sub> nanozymes for Ce 3d. **D, E)** XPS spectra of Cr/CeO<sub>2</sub> nanozyme for Ce 3d, and Cr 2p, respectively. **F)** Ratio of Ce<sup>3+</sup>/Ce<sup>4+</sup> in CeO<sub>2</sub> and Cr/CeO<sub>2</sub> nanozymes. **G)** HRTEM image of Cr/CeO<sub>2</sub> nanozyme. **H)** STEM-EDX mapping images of Cr/CeO<sub>2</sub> nanozyme.

## Optimization of catalytic activity

To investigate catalytic properties, the differences in catalytic performance of CeO<sub>2</sub> nanozymes doped with different metal elements (such as Ag, Cr, Co, Rh, Pd, Mn, Ni) were first explored. As show in **Figure 2A-B**, the CeO<sub>2</sub> nanozyme exhibits the best catalytic activity when Cr is doped. Then, a series of Cr/CeO<sub>2</sub> nanozymes at different doping ratios were synthesized. The CeO<sub>2</sub> nanozymes with different doping were subjected to a comparative test of POD-like activity. It is noting that Cr/CeO<sub>2</sub> nanozyme at 10% doping concentration exhibits the best POD-like activity among all samples (**Figure 2C-D**). Moreover, the results of XPS spectra show that the Ce<sup>3+</sup>/Ce<sup>4+</sup> ratio of Cr/CeO<sub>2</sub> nanozyme is the highest at 10% doping concentration (**Figure S2**), which indicates that the main reason for the enhancement of POD-like activity of Cr/CeO<sub>2</sub> nanozyme is the increase of Ce<sup>3+</sup>/Ce<sup>4+</sup> ratio caused by Cr<sup>3+</sup> doping. Thus, the Cr/CeO<sub>2</sub> nanozyme at 10% doping concentration was selected as the research object for further exploration. In addition, the typical

Michaelis–Menten curves were performed for Cr/CeO<sub>2</sub> nanozyme (**Figure 2E-F**) and HRP (**Figure S3**). To further analyze the catalytic mechanism, steady-state kinetic parameters for the oxidation of TMB in present of H<sub>2</sub>O<sub>2</sub> were also calculated. The  $V_{max}$  and  $K_m$  were obtained using Lineweaver–Burk plot and are shown in **Table 1**. The  $K_m$  value of Cr/CeO<sub>2</sub> nanozyme with H<sub>2</sub>O<sub>2</sub> as the substrate is in the same order of magnitude as that of HRP. The  $K_m$  value of Cr/CeO<sub>2</sub> nanozyme with TMB as substrate is significantly lower than that of HRP, indicating that Cr/CeO<sub>2</sub> nanozyme possesses higher affinity to TMB than HRP.

**Table 1.** Comparison of the Michaelis–Menten constant ( $K_m$ ) and maximum reaction rate ( $V_{max}$ ) between Cr/CeO<sub>2</sub> nanozyme and HRP.

Nanozyme	Substance	$K_m$ [mM]	$V_{max}$ [ $\mu\text{M/s}$ ]
Cr/CeO <sub>2</sub>	TMB	0.080±0.009	0.138±0.027
Cr/CeO <sub>2</sub>	H <sub>2</sub> O <sub>2</sub>	0.867±0.073	0.159±0.024
HRP	TMB	0.200±0.042	0.124±0.023
HRP	H <sub>2</sub> O <sub>2</sub>	0.665±0.063	0.112±0.016

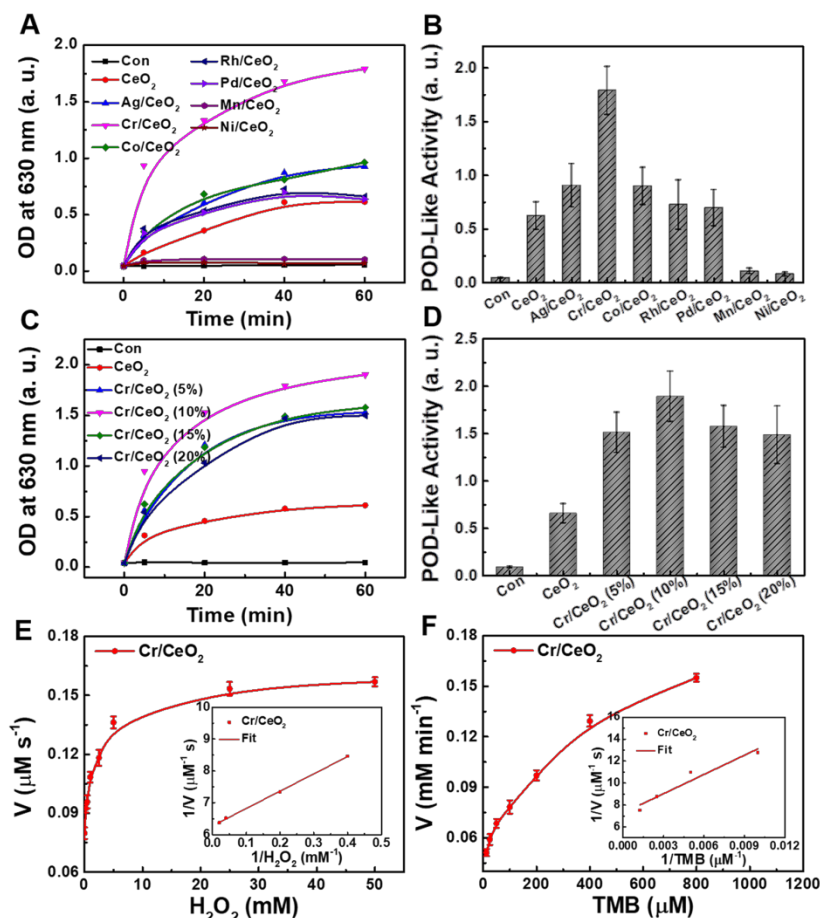


**Figure 2. Optimization of catalytic activity.** **A)** Time-dependent absorbance of CeO<sub>2</sub> nanozymes doped with different metal elements at 630 nm in TMB method. **B)** POD-like activity of CeO<sub>2</sub> nanozymes doped with different metal elements. **C)** Time-dependent absorbance of Cr/CeO<sub>2</sub> nanozymes with different doping ratios at 630 nm in TMB method. **D)** POD-like activity of Cr/CeO<sub>2</sub> nanozymes with different doping ratios. Deionized water serves as blank control in all assay, marked as "con". The velocity ( $v$ ) of the reaction was measured by steady-state kinetic assay using 50  $\mu\text{g/mL}$  Cr/CeO<sub>2</sub> nanozyme. **E)** The concentration of TMB was 0.8 mM and varied concentration of H<sub>2</sub>O<sub>2</sub>. **F)** The concentration of H<sub>2</sub>O<sub>2</sub> was 50 mM and varied concentration of TMB. Inset: Double-reciprocal plots of activity of Cr/CeO<sub>2</sub> nanozyme at a fixed concentration of one substrate versus varying concentration of the second substrate.

### Multienzyme-like activity evaluation

Based on the results of the catalytic activity in the above exploration, the multienzyme-like property of Cr/CeO<sub>2</sub> nanozyme was further studied. **Figure 3A-B** reveal the POD-like activity of the Cr/CeO<sub>2</sub> nanozyme (10% doping) approximately 3-4 times higher than that of CeO<sub>2</sub>, identifying the improvement of catalytic property. In addition, in order to evaluate the stability of Cr/CeO<sub>2</sub> nanozyme,

the Cr/CeO<sub>2</sub> nanozyme was put in DMEM for one month. Then, the POD-like activity and structure of initial and old Cr/CeO<sub>2</sub> nanozyme were evaluated. As shown in **Figure S4**, there is no significant difference in the chemical state of Cr between initial Cr/CeO<sub>2</sub> and old Cr/CeO<sub>2</sub> nanozyme in performance and structure, which illustrates the excellent stability of Cr/CeO<sub>2</sub> nanozyme.

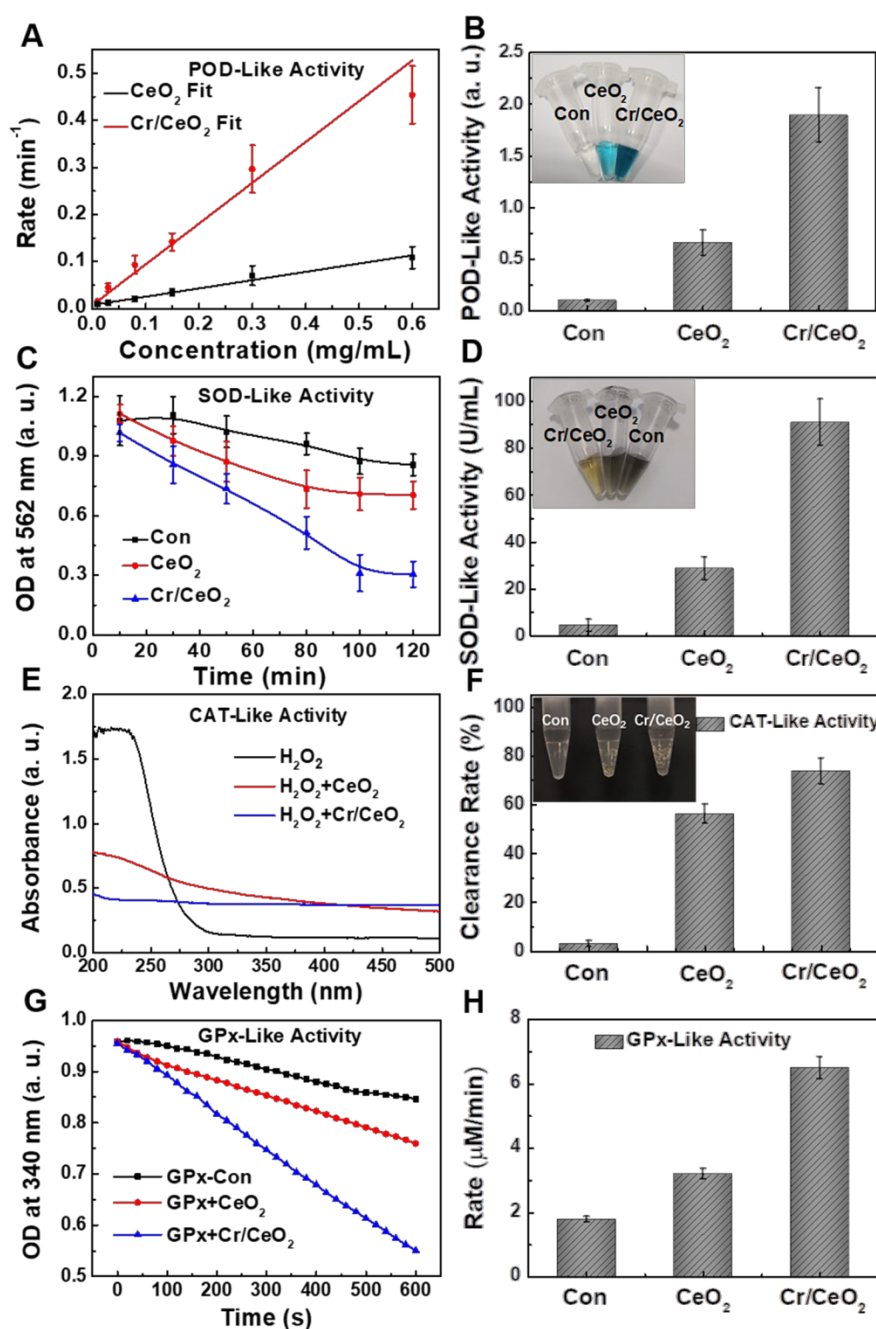


**Figure 3. Multienzyme-like activity of Cr/CeO<sub>2</sub> nanozyme.** **A)** Concentration-dependent reaction rate for Cr/CeO<sub>2</sub> nanozyme in TMB Assay. **B)** POD-like activity of Cr/CeO<sub>2</sub> nanozyme. Inset: Photo images of final solution after reacting with Cr/CeO<sub>2</sub> nanozymes for 60 min in TMB method. **C)** Time-dependent absorbance at 562 nm with Cr/CeO<sub>2</sub> nanozyme in NBT method. **D)** SOD-like activity of Cr/CeO<sub>2</sub> nanozyme. Inset: Photo images of result solution after reacting with Cr/CeO<sub>2</sub> nanozymes for 140 min in NBT method. **E)** Absorbance of H<sub>2</sub>O<sub>2</sub> solution with or without Cr/CeO<sub>2</sub> nanozyme. **F)** H<sub>2</sub>O<sub>2</sub> clearance rate of Cr/CeO<sub>2</sub> nanozyme. Inset: Photo images of H<sub>2</sub>O<sub>2</sub> solution after reacting with Cr/CeO<sub>2</sub> nanozyme for 10 min. **G)** GPx-like activity of Cr/CeO<sub>2</sub> nanozyme by GPx Assay Kit. **H)** Corresponding reaction rate of Cr/CeO<sub>2</sub> nanozyme was calculated during GPx-like activity assay. Deionized water serves as blank control in all assay, marked as "con".

Moreover, the SOD-like activity of Cr/CeO<sub>2</sub> nanozyme was assessed by classical NBT chromogenic method. **Figure 3C** shows that the absorbance at 560 nm changes with reaction time after the uptake of Cr/CeO<sub>2</sub> nanozyme, indicating efficient SOD-like activity. Quantitative results in **Figure 3D** exhibit the SOD-like activity of Cr/CeO<sub>2</sub> nanozyme is about 3 times higher than that of CeO<sub>2</sub>. Meanwhile, the SOD-like activity of the Cr/CeO<sub>2</sub> nanozyme increases almost linearly relative to its concentration (**Figure S5**). Subsequently, the CAT-like activity was determined by comparing the decrease in the absorbance of H<sub>2</sub>O<sub>2</sub> at 240 nm when CeO<sub>2</sub> or Cr/CeO<sub>2</sub> nanozymes were separately added. A significant decrease in the absorbance of H<sub>2</sub>O<sub>2</sub> with Cr/CeO<sub>2</sub> is observed, and the clearance rate of H<sub>2</sub>O<sub>2</sub> is 75%, obviously higher than CeO<sub>2</sub> (**Figure 3E-F**). In addition, the CAT-like activity of Cr/CeO<sub>2</sub> nanozyme in neutral and alkaline environment is better than the level of acid environment, but comparable to the activity in inflammatory environment (**Figure S6**). Similarly, the GPx-like activity of Cr/CeO<sub>2</sub> was investigated by detecting the evolution in absorbance of NADPH at 340 nm according to the classical glutathione reductase coupling reaction mechanism. As show in **Figure 3G-H**, the GPx-like activity of the Cr/CeO<sub>2</sub> nanozyme turn a significant enhancement compared to CeO<sub>2</sub>, with a reaction rate of 6.5 μmol L<sup>-1</sup> min<sup>-1</sup>. **Figure S7** reveals that the reaction rate is also proportional to the concentration of nanozyme, suggesting the good GPx-like activity. In addition, the CAT-like, GPx-like and SOD-like activities of nanozyme with different doping metal elements and different Cr-doping concentrations were also investigated. The results show that the CeO<sub>2</sub> nanozyme with 10% Cr-doping exhibits the optimal multienzyme-like activity (**Figure S8**). Importantly, the pure CeO<sub>2</sub> nanozyme mainly exhibits SOD-like and CAT-like enzyme activities, consistent with previous reports in the literature [50-54], while as-obtained Cr/CeO<sub>2</sub> nanozyme is capable of simulating three major antioxidant enzymes, including SOD, CAT and GPx, due to the incorporation of Cr<sup>3+</sup> ions. Thereby, Cr/CeO<sub>2</sub> nanozyme is expected to play an important role in intracellular antioxidants by the synergistic effect of multienzyme-like properties, maintaining intracellular redox homeostasis.

### RONS scavenging capacities of Cr/CeO<sub>2</sub> nanozyme

Furthermore, to determine the free radicals scavenging abilities of the Cr/CeO<sub>2</sub> nanozyme, the ESR spectroscopy was performed. As show in **Figure 4A-B**, the ESR signals are significantly reduced after

adding Cr/CeO<sub>2</sub> nanozyme, indicating the scavenging rate to •OH and O<sub>2</sub><sup>•-</sup> free radicals. The nanozyme displays the higher sensitivity to •OH than O<sub>2</sub><sup>•-</sup> at same concentration (**Figure 4C**). For reactive nitrogen species (RNS) scavenging, the total RNS level has improved, but it remains to be enhanced. The Cr/CeO<sub>2</sub> nanozyme prefers to clean up ONOO<sup>-</sup> with a clearance rate as high as 93%, and the clearing of •NO is only 57%, but still obviously higher than that of CeO<sub>2</sub> (**Figure 4D-E**). Moreover, the results reveal that the ONOO<sup>-</sup>-scavenging performance of Cr/CeO<sub>2</sub> nanozyme in neutral environments is better than that of alkaline environments (**Figure S9**). The DPPH radical acts as a very stable nitrogen-centered free radical due to its specific structure with three benzene rings. The clearance rate of Cr/CeO<sub>2</sub> nanozyme against DPPH is improved to 50%, which is 2.5 times that of undoped CeO<sub>2</sub> (**Figure 4F**). Therefore, it has been demonstrated that the Cr doping can enhance the free radicals scavenging ability to multiple RONS, which is vital for preventing oxidative damage in biosystem. In particular, the ability of Cr/CeO<sub>2</sub> nanozyme to selectively purify RNS, an important signaling molecules in the brain, was rarely reported before [55-57]. This result makes it highly potential for the treatment of brain injury.

### In vitro cytotoxicity and free radical detection

Inspired by the above work, the survival rate of injured neuron cells after nanozyme treatment was detected firstly to evaluate the *in vitro* free radicals scavenging abilities of Cr/CeO<sub>2</sub> nanozyme. The results show high cellular viability to HT22 cells within the nanozyme doses of 100 μg/mL (**Figure 5A**), illustrating low cytotoxicity of Cr/CeO<sub>2</sub> nanozyme. Then, the LPS were used to stimulate the cells, and the survival rate of HT22 cells decreased to 80%, indicating obvious toxicity after 24 h uptake. However, the viabilities of injured cells are improved gradually under the treatment of Cr/CeO<sub>2</sub> nanozymes with different concentrations (**Figure 5B**). Meanwhile, the total ROS, O<sub>2</sub><sup>•-</sup> and •NO levels induced by LPS in the presence or absence of Cr/CeO<sub>2</sub> nanozyme treatment were monitored using DCFH-DA, DHE and DAF-FM DA probes. As show in **Figure 5C-D**, both flow cytometry and fluorescence images exhibit the same trend for RONS. For the total ROS, it can be seen that fluorescence intensity of injured cells enhances after incubation of LPS, indicating RONS production. The fluorescence intensity decreases after nanozyme treatment, and the reduction of Cr/CeO<sub>2</sub> nanozyme is more significant than that of undoped CeO<sub>2</sub>. As for O<sub>2</sub><sup>•-</sup> and •NO, the change of fluorescence intensity is basically consistent with ROS. The results suggest that Cr/CeO<sub>2</sub>

nanozyme can remove RONS and prevent cells from the oxidative damage induced by LPS. Under the stimulation of LPS, intracellular RONS levels are rapidly elevated, resulting in damage to DNA, protein

and lipids [58-59]. Crucially, it is proved that Cr/CeO<sub>2</sub> nanozyme can improve the survival rate of neuron cells by eliminating oxidative stress induced by RONS.

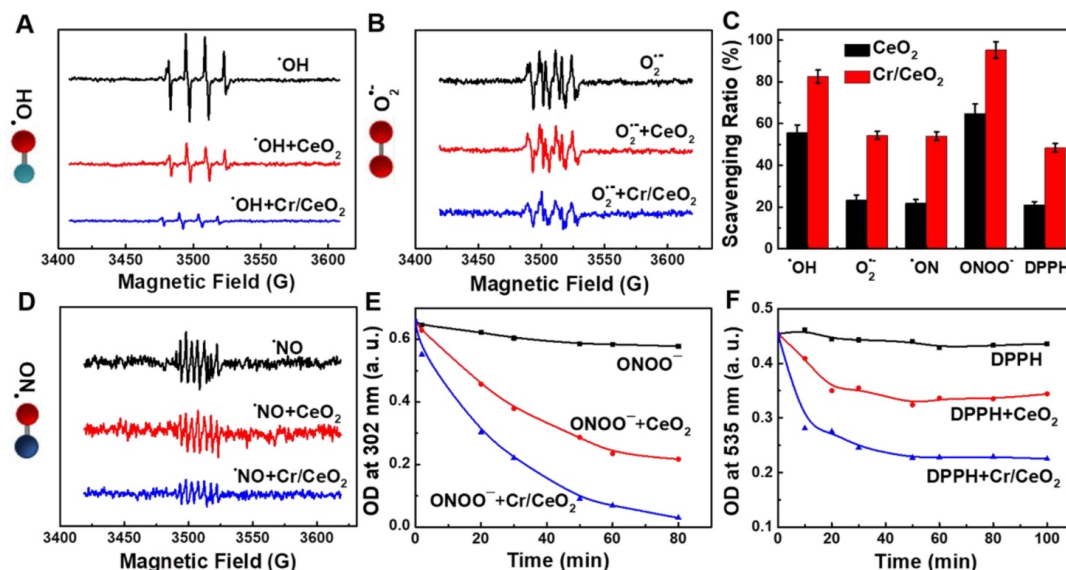


**Figure 4.** RONS scavenging selectively of Cr/CeO<sub>2</sub> nanozyme. ROS scavenging abilities of the Cr/CeO<sub>2</sub> nanozyme for **A)** ·OH and **B)** O<sub>2</sub><sup>·-</sup> tested by ESR, respectively. **C)** Comparison of the ability of Cr/CeO<sub>2</sub> nanozymes to scavenge free radicals for ·OH, O<sub>2</sub><sup>·-</sup>, ·NO, ONOO<sup>-</sup> and DPPH. RNS scavenging abilities of the Cr/CeO<sub>2</sub> nanozyme for **D)** ·NO, **E)** ONOO<sup>-</sup> and **F)** DPPH tested by ESR and UV-vis absorption spectra, respectively.

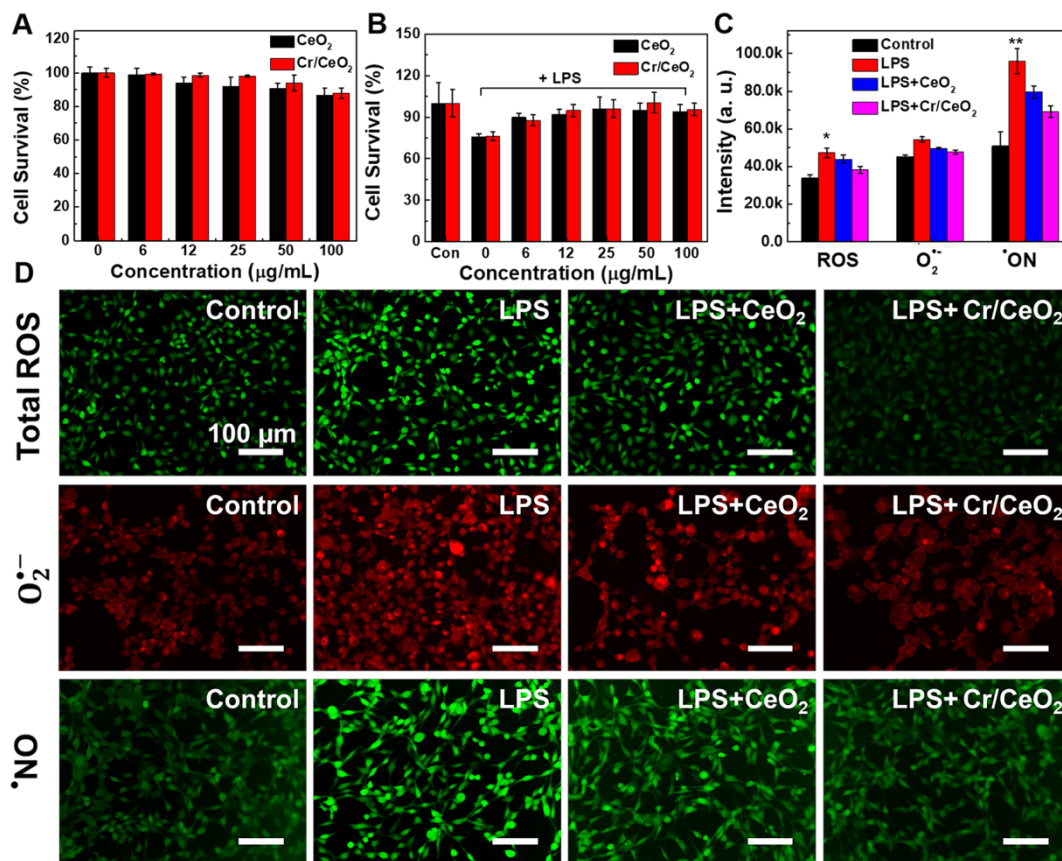


**Figure 5.** In vitro treatment of Cr/CeO<sub>2</sub> nanozyme. **A)** Cell survival of HT22 cells treated with different concentrations of Cr/CeO<sub>2</sub> nanozyme measured by MTT assay. **B)** Cell survival of LPS induced HT22 cells treated with different concentrations of Cr/CeO<sub>2</sub> nanozyme measured by MTT assay. **C)** The corresponding quantitative analysis by a flow cytometer and **D)** fluorescence images of total ROS, O<sub>2</sub><sup>·-</sup> and ·NO levels in HT22 cells induced by LPS in the presence or absence of Cr/CeO<sub>2</sub> nanozyme were measured using DCFH-DA, DHE and DAF-FM DA probes, respectively. Asterisks indicate significant differences (\*P < 0.05, \*\*P < 0.01, \*\*\*P < 0.001) as compared with the control group, analyzed by a Student's t test.

## TBI treatment by Cr/CeO<sub>2</sub> nanozyme catalytic patch

The multienzyme-like activity of Cr/CeO<sub>2</sub> nanozyme *in vitro* encourage us to explore the *in vivo* TBI treatment of nanozymes in noninvasive route. In order to minimize toxicity and side effects, a Cr/CeO<sub>2</sub> nanozyme patch is developed to treat TBI. As show in **Figure 6A**, catalytic patch is based on Cr/CeO<sub>2</sub> nanozyme, and the porous nickel foams as supporting materials. **Figure 6B** reveals the Cr/CeO<sub>2</sub> nanozyme still possesses high catalytic activity after forming nanozyme patch, and the antioxidant properties of the catalytic patch did not diminish after one month (**Figure 6C**), proving good stability. The C57 mice aged 6-8 weeks were established in TBI model, and were randomly divided into three groups ( $n = 13$  in each group). The wound sizes of mice in all three groups were measured every other day. The wounds of mice with Cr/CeO<sub>2</sub> nanozyme patch treatment show almost complete healing on the 8th day, and wounds of mice in TBI group exhibit slow recovery (**Figure 6D** and **S10**). Besides, the body weights of

mice in TBI+Cr/CeO<sub>2</sub> group also grow faster than that of mice in TBI group (**Figure 6E**). Furthermore, the concentration and diffusion depth of Cr/CeO<sub>2</sub> nanozyme released from the patch into brain tissue through the injured site were monitored by ICP-MS. The results show that the Cr/CeO<sub>2</sub> nanozyme released from the patch and spread into the brain tissue through the injury location within 6 hours after brain injury (**Figure S11**). After TBI injury, the blood-brain barrier (BBB) is in the open state for a short time, and the Cr/CeO<sub>2</sub> nanozyme released from the patch can pass through the BBB and spread into the brain tissue. Therefore, the topical treatment based on Cr/CeO<sub>2</sub> nanozyme patch accelerates wound healing, which is in agreement with earlier report that oxidative stress in the microenvironment of wound site is alleviated by inhibiting ROS levels [60-62], and relieves the effects of brain injury in body weight. It is speculated that these results potentially have a potential therapeutic effects on the recovery of brain tissue levels in TBI.

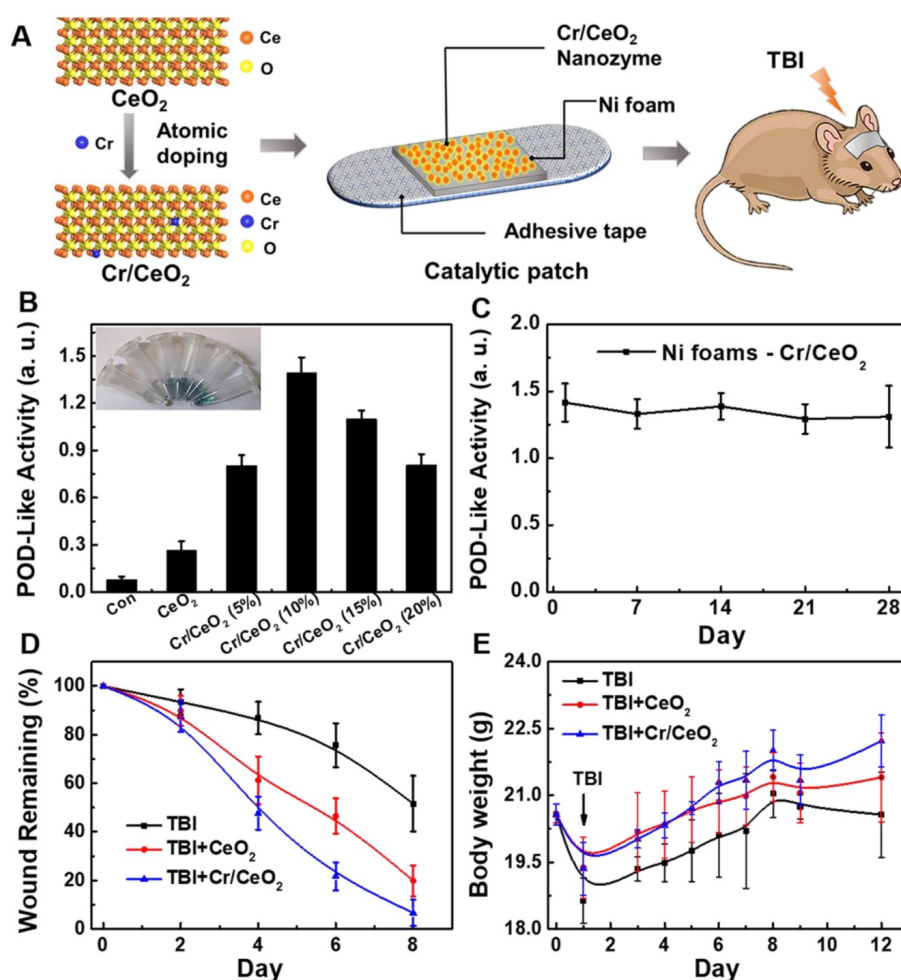


**Figure 6.** Design of nanozyme patch and TBI treatment. **A**) Design of catalytic patch base on Cr/CeO<sub>2</sub> nanozyme for TBI treatment. **B**) POD-like activity of catalytic patch base on Cr/CeO<sub>2</sub> nanozyme with different doping. **C**) Stability of Cr/CeO<sub>2</sub> nanozyme patch at 10% doping concentration. **D**) Wound length of mice in the presence or absence of nanozyme patch treatment after TBI. **E**) Body weight of mice with or without nanozyme patch treatment after TBI.

To further understand the effect of Cr/CeO<sub>2</sub> nanozyme patch on cerebral oxidative stress-induced neuronal responses, immunofluorescence staining of the brain sections was carried out to observe the difference among the brain injured mice with or without patch treatment. The morphology and number of astrocytes and microglia in **Figure 7** are analyzed. When mice are subjected to brain injury, a large number of astrocytes and microglia are activated by the acute immune response, and the treatment of nanozyme patch can remarkably decrease the neuroinflammation (**Figure 7A-B**). Similarly, MMP-9, a pro-inflammatory factor, is also a biomarker for testing inflammation in the brain. The MMP-9 shows high expression level following TBI, but it reduces sharply after nanozyme patch treatment (**Figure 7C**). Quantitative analyses of the difference in

immunofluorescence also confirm that the treatment of Cr/CeO<sub>2</sub> nanozyme patch can improve the neurons loss in brain tissue following TBI, alleviating neuroinflammation [63-65] (**Figure 7D**). Additionally, elevated levels of RONS cause an increase in lipid peroxidation and inhibit the activity of SOD in the brain. The results reveal that the lipid peroxidation from the brain tissue can be increased and SOD activity can be decreased within 12 days after TBI. Whereas the treatment with nanozyme patch reduces lipid peroxidation and increases the SOD activity (**Figure 7E-F**). Thereby, it is further confirmed that the nanozyme patch-based topical treatment is an effective route for alleviating excessive oxidative stress in the brain and improving physiological environment of nerve cells.

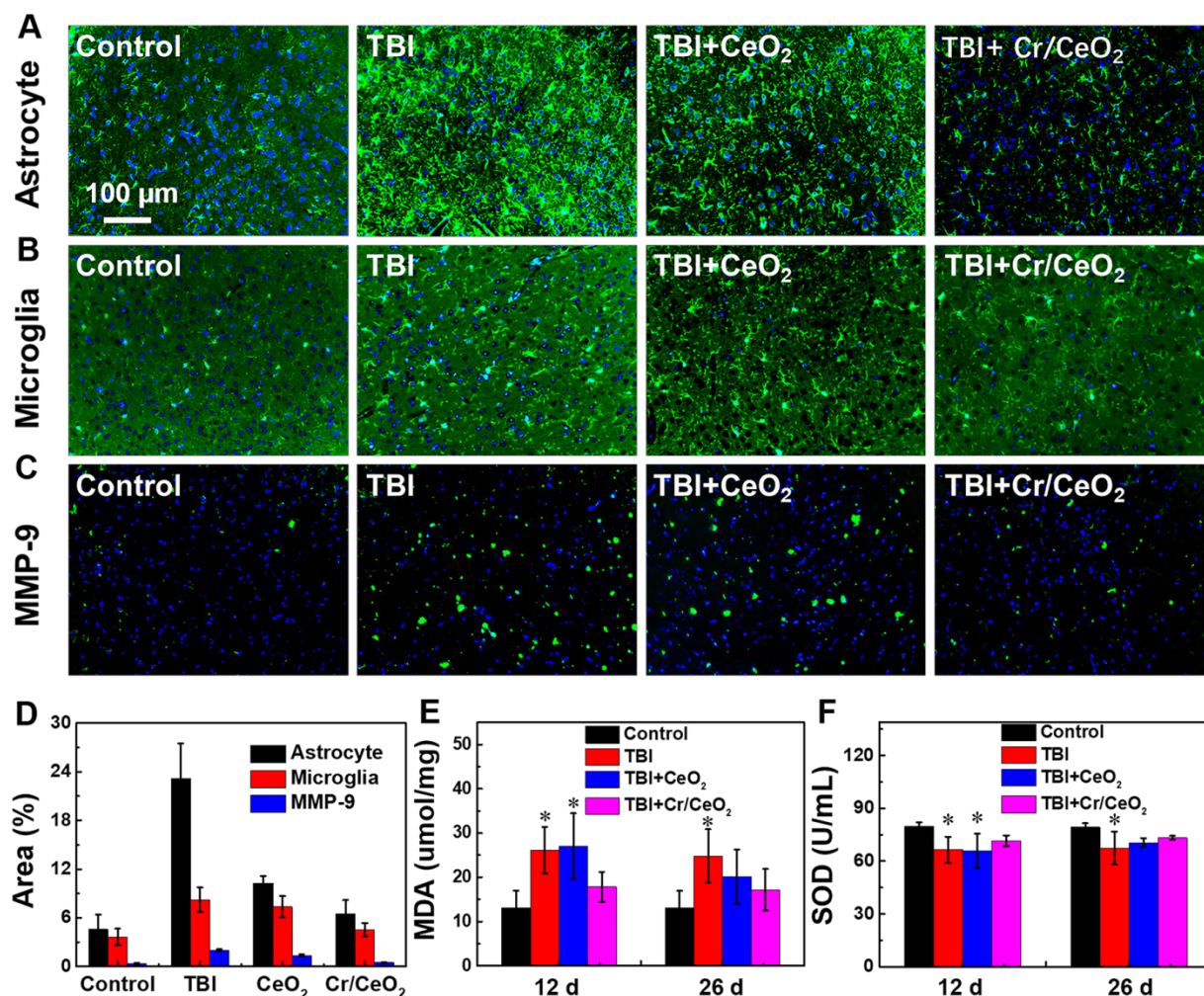


**Figure 7.** *In vivo* treatment of Cr/CeO<sub>2</sub> nanozyme. **A-C**) Immunostaining image of astrocytes, microglia and MMP-9 of the brain sections at 12 days after injury were detected using anti-GFAP, anti-Iba-1 and anti-MMP-9, respectively. **D**) Corresponding analysis of astrocytes, microglia and MMP-9 based on the immunostaining image were calculated by ImageJ software. **E**) MDA levels in brain tissue was tested at 12 and 26 days after injury. **F**) SOD activity was quantified at 12 and 26 days after injury. All tests were performed on four groups: healthy control, TBI, TBI+CeO<sub>2</sub> and TBI+Cr/CeO<sub>2</sub> nanozyme patch. Asterisks indicate significant differences (\*P < 0.05, \*\*P < 0.01, \*\*\*P < 0.001) as compared with the control group, analyzed by a Student's t test.

## Behavior test

Finally, morris water maze test was performed to investigate spatial learning ability and memory ability of mice. **Figure 8A** shows that most of mice in all groups are unable to find the platform when they are trained on the first day. After 5 days of training, normal mice are able to quickly locate and land on the platform. The mice with Cr/CeO<sub>2</sub> nanozyme patch treatment can successfully find the platform after a short period of time, while the mice in TBI group still do not quickly locate the exact position of platform. **Figure 8B-C** show that nanozyme patch-treated mice shorten the time for searching platform and stay closer to the platform during the 5-day training period, indicating that the mice after treatment have better learning ability compared with injured mice. Analyses of swimming speed of mice reveal that the mice with the treatment of Cr/CeO<sub>2</sub> nanozyme patch are faster and closer to health mice (**Figure 8D**). After

the platform is removed on the fifth day, the mice treated with nanozyme patch are able to quickly find and return to the location of the previous platform multiple times (**Figure 8E-F**). Therefore, behavioral testing demonstrates that the neuronal cognition of mice treated with nanozyme patch is improved, and their spatial learning and memory abilities are close to healthy mice. Finally, the blood chemistry and biochemical analysis were conducted on mice treated with or without nanozyme patch at 12 and 26 days post TBI, respectively, and compared with healthy mice. **Figure S12** and **S13** reveal that the mice treated with nanozyme patch have alleviated the abnormality of blood chemistry caused by TBI. Therefore, it can be seen that the administration mode of topical treatment has proven its feasibility in terms of safety and convenience, providing a promising noninvasive solution for future TBI treatment.

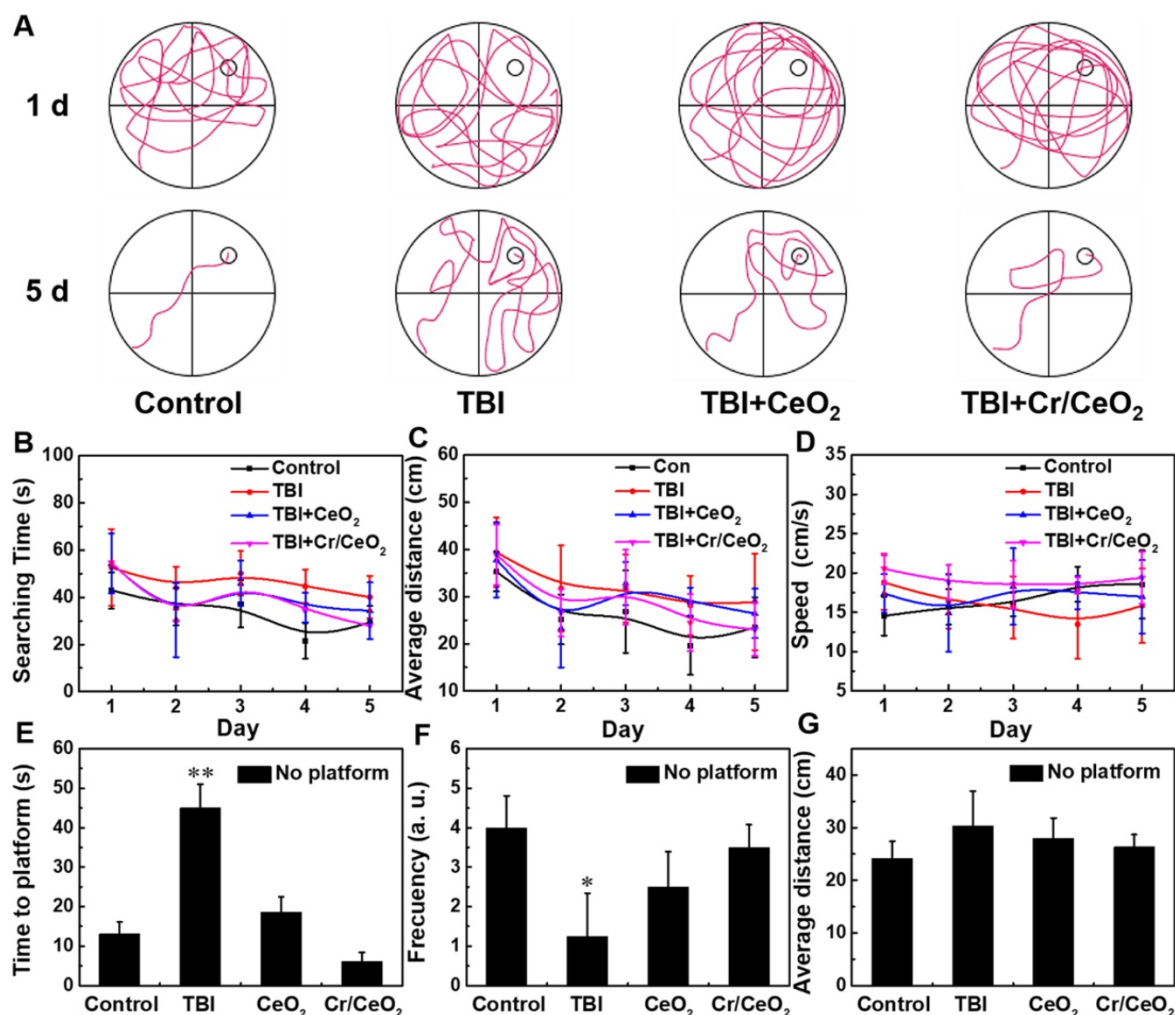


**Figure 8. Behavioral tests after TBI.** **A)** Path of the mice search platform in training on the first and fifth days. **B)** Time for searching the platform, **C)** average distance to platform, and **D)** swimming speed of mice during 5 days training. **E)** Time to find the initial hidden platform area for the first time, **F)** frequency of reaching the hidden platform area, and **G)** average distance from mice to the hidden platform area after the platform is removed on the fifth day test. All tests were performed on four groups: healthy control, TBI, TBI+CeO<sub>2</sub> and TBI+ Cr/CeO<sub>2</sub> nanozyme patch. Asterisks indicate significant differences (\*P < 0.05, \*\*P < 0.01, \*\*\*P < 0.001) as compared with the control group, analyzed by a Student's t test.

Nowadays, traditional treatments mainly performed by tail vein injection or intraperitoneal injection through the blood circulation [18, 66-69], accompanied by potential biosafety issues associated with the inherent toxicity of nanomaterials. It is essential to explore a new type of TBI treatment to reduce side effects. Herein, catalytic patch based on redox Cr/CeO<sub>2</sub> nanozyme, a noninvasive topical treatment mode, was developed to fulfill this goal, significantly diminishing the accumulation of nanozyme in the brain without affecting its therapeutic effect. At the same time, the potential toxicity caused by doping of chromium, which is greatly reduced via this noninvasive treatment method. Moreover, the catalytic activity of previously reported ceria nanozyme is still not high enough, and the free radicals scavenging abilities are primarily directed to ROS [41]. In this work, the obtained Cr/CeO<sub>2</sub> nanozyme with multienzyme-like activities and possesses more removal affinity towards RNS, especially ONOO<sup>-</sup> and DPPH, the secondary RNS with high reactivity and neurotoxicity [11]. Therefore, it is desirable to promote the application of nanozyme patch into clinical therapeutic, including *in vivo* inflammation treatment, by increasing the biocompatibility of substrate materials. Furthermore, efforts will be focused on synthesis ultra-small size nanozyme at atomic precision levels to further elevate its GPx-like performance and the ability to selectively remove free radicals [70-75].

## Conclusion

In summary, the catalytic patch based on redox Cr/CeO<sub>2</sub> nanozyme is developed for TBI therapy. The catalytic activity of nanozyme is optimized by modulating Cr<sup>3+</sup> doping ratio. The Cr/CeO<sub>2</sub> nanozyme possesses more effective RONS scavenging and multienzyme-like properties than undoped ceria, which is ascribed to the increase of Ce<sup>3+</sup>/Ce<sup>4+</sup> ratio. *In vitro* experiments reveal the Cr/CeO<sub>2</sub> nanozyme exhibits protection effects of cells against by LPS- and H<sub>2</sub>O<sub>2</sub>-induced damage. Meanwhile, *in vivo* experiments suggest that the nanozyme patch accelerates wound healing by improving SOD activity and reducing lipid peroxide. Tissue staining indicates that the treatment with nanozyme patch relieves excessive stress response of nerve cells in the brain. Furthermore, behavior test proves mice with nanozyme patch treatment exhibit strikingly neurocognitive recovery in spatial learning and memory abilities. Present work provides a noninvasive TBI therapeutic approach of nanozyme patch with minimized side effects.

## Supplementary Material

Supplementary figures.

<http://www.thno.org/v11p2806s1.pdf>

## Acknowledgements

This work was financially supported by the National Natural Science Foundation of China (Grant Nos. 91859101, 81971744, U1932107, 81471786 and 82001952) and National Natural Science Foundation of Tianjin (Nos. 19JCZDJC34000 and 20JCYBJC00940), the Innovation Foundation of Tianjin University.

## Competing Interests

The authors have declared that no competing interest exists.

## References

- Ghajar J. Traumatic brain injury. *The Lancet*. 2000; 356: 923-929.
- Langlois JA, Rutland-Brown W, Wald MM. The epidemiology and impact of traumatic brain injury: A brief overview. *J Head Trauma Rehab*. 2006; 21: 375-378.
- Cornelius C, Crupi R, Calabrese V, Graziano A, Milone P, Pennisi G, et al. Traumatic brain injury: Oxidative stress and neuroprotection. *Antioxid Redox Sign*. 2013; 19: 836-853.
- Roozenbeek B, Maas AI, Menon DK. Changing patterns in the epidemiology of traumatic brain injury. *Nat Rev Neurol*. 2013; 9: 231-236.
- Slemmer JE, Shacka JJ, Sweeney M, Weber JT. Antioxidants and free radical scavengers for the treatment of stroke, traumatic brain injury and aging. *Curr Med Chem*. 2008; 15: 404-414.
- Corps KN, Roth TL, McGavern DB. Inflammation and neuroprotection in traumatic brain injury. *JAMA Neurol*. 2015; 72: 355-362.
- Abdul-Muneer PM, Chandra N, Haorah J. Interactions of oxidative stress and neurovascular inflammation in the pathogenesis of traumatic brain injury. *Mol Neurobiol*. 2015; 51: 966-979.
- Shlosberg D, Benifla M, Kaufer D, Friedman A. Blood-brain barrier breakdown as a therapeutic target in traumatic brain injury. *Nat Rev Neurol*. 2010; 6: 393-403.
- Russo MV, McGavern DB. Inflammatory neuroprotection following traumatic brain injury. *Science*. 2016; 353: 783-785.
- Block ML, Zecca L, Hong J-S. Microglia-mediated neurotoxicity: Uncovering the molecular mechanisms. *Nat Rev Neurosci*. 2007; 8: 57-69.
- Hagberg H, Mallard C, Ferriero DM, Vannucci SJ, Levison SW, Vexler ZS, et al. The role of inflammation in perinatal brain injury. *Chem Commun (Camb)*. 2015; 11: 192-208.
- Kelm M, Dahmann R, Wink D, Feelisch M. The nitric oxide/superoxide assay insights into the biological chemistry of the NO/O<sub>2</sub> interaction. *J Biol Chem*. 1997; 272: 9922-9932.
- Bains M, Hall ED. Antioxidant therapies in traumatic brain and spinal cord injury. *BBA-Mole Basis Dis*. 2012; 1822: 675-684.
- Xu J, Ypma M, Chiarelli PA, Park J, Ellenbogen RG, Stayton PS, et al. Theranostic oxygen reactive polymers for treatment of traumatic brain injury. *Adv Funct Mater*. 2016; 26: 4124-4133.
- Yoo D, Magsam AW, Kelly AM, Stayton PS, Kievit FM, Convertine AJ. Core-cross-linked nanoparticles reduce neuroinflammation and improve outcome in a mouse model of traumatic brain injury. *ACS Nano*. 2017; 11: 8600-8611.
- Wei H, Wang E. Nanomaterials with enzyme-like characteristics (nanozymes): Next-generation artificial enzymes. *Chem Soc Rev*. 2013; 42: 6060-6093.
- Huang Y, Liu Z, Liu C, Ju E, Zhang Y, Ren J, et al. Self-assembly of multi-nanozymes to mimic an intracellular antioxidant defense system. *Angew Chem Int Ed*. 2016; 55: 6646-6650.
- Mu X, Wang J, Li Y, Xu F, Long W, Ouyang L, et al. Redox trimetallic nanozyme with neutral environment preference for brain injury. *ACS Nano*. 2019; 13: 1870-1884.
- Manickam DS, Brynskikh AM, Kopanic JL, Sorgen PL, Klyachko NL, Batrakova EV, et al. Well-defined cross-linked antioxidant nanozymes for treatment of ischemic brain injury. *J Control Release*. 2012; 162: 636-645.
- Hao C, Qu A, Xu L, Sun M, Zhang H, Xu C, et al. Chiral molecule-mediated porous Cu<sub>2</sub>O nanoparticle clusters with antioxidant activity for ameliorating parkinson's disease. *J Am Chem Soc*. 2018; 141: 1091-1099.
- Zhang Z, Zhang X, Liu B, Liu J. Molecular imprinting on inorganic nanozymes for hundred-fold enzyme specificity. *J Am Chem Soc*. 2017; 139: 5412-5419.
- Lin Y, Ren J, Qu X. Nano-gold as artificial enzymes: Hidden talents. *Adv Mater*. 2014; 26: 4200-4217.

23. Chen F, Bai M, Cao K, Zhao Y, Wei J, Zhao Y. Fabricating MnO<sub>2</sub> nanozymes as intracellular catalytic DNA circuit generators for versatile imaging of base-excision repair in living cells. *Adv Funct Mater.* 2017; 27: 1702748.
24. Wang H, Wan K, Shi X. Recent advances in nanozyme research. *Adv Mater.* 2018; e1805368.
25. Tao Y, Ju E, Ren J, Qu X. Bifunctionalized mesoporous silica-supported gold nanoparticles: Intrinsic oxidase and peroxidase catalytic activities for antibacterial applications. *Adv Mater.* 2015; 27: 1097-1104.
26. Wang JY, Mu X, Li Y, Xu F, Long W, Yang J, et al. Hollow ptpdrh nanocubes with enhanced catalytic activities for *in vivo* clearance of radiation-induced ROS via surface-mediated bond breaking. *Small.* 2018; 14: e1703736.
27. Liu Z, Wang F, Ren J, Qu X. A series of MOF/Ce-based nanozymes with dual enzyme-like activity disrupting biofilms and hindering recolonization of bacteria. *Biomaterials.* 2019; 208: 21-31.
28. Huang Y, Ren J, Qu X. Nanozymes: Classification, catalytic mechanisms, activity regulation, and applications. *Chem Rev.* 2019; 119: 4357-4412.
29. Zhou Y, Liu B, Yang R, Liu J. Filling in the gaps between nanozymes and enzymes: Challenges and opportunities. *Bioconjug Chem.* 2017; 28: 2903-2909.
30. Liu X, Gao Y, Chandrawati R, Hosta-Rigau L. Therapeutic applications of multifunctional nanozymes. *Nanoscale.* 2019; 11: 21046-21060.
31. Gao L, Fan K, Yan X. Iron oxide nanozyme: A multifunctional enzyme mimetic for biomedical applications. *Theranostics.* 2017; 7: 3207-3227.
32. Zhao S, Yu X, Qian Y, Chen W, Shen J. Multifunctional magnetic iron oxide nanoparticles: An advanced platform for cancer theranostics. *Theranostics.* 2020; 10: 6278-6309.
33. Di H, Mi Z, Sun Y, Liu X, Liu X, Li A, et al. Nanozyme-assisted sensitive profiling of exosomal proteins for rapid cancer diagnosis. *Theranostics.* 2020; 10: 9303-9314.
34. Jiang B, Fang L, Wu K, Yan X, Fan K. Ferritins as natural and artificial nanozymes for theranostics. *Theranostics.* 2020; 10: 687-706.
35. Wang X, Cao W, Qin L, Lin T, Chen W, Lin S, et al. Boosting the peroxidase-like activity of nanostructured nickel by inducing its 3+ oxidation state in lanio(3) perovskite and its application for biomedical assays. *Theranostics.* 2017; 7: 2277-2286.
36. Vernekar AA, Sinha D, Srivastava S, Paramasivam PU, D'Silva P, Mughes G. An antioxidant nanozyme that uncovers the cytoprotective potential of vanadia nanowires. *Nat Commun.* 2014; 5: 5301.
37. Ghosh S, Roy P, Karmodak N, Jemmis ED, Mughes G. Nanoisozymes: Crystal-facet-dependent enzyme-mimetic activity of V<sub>2</sub>O<sub>5</sub> nanomaterials. *Angew Chem Int Ed.* 2018; 57: 4510-4515.
38. André R, Natálio F, Humanes M, Leppin J, Heinze K, Wever R, et al. V<sub>2</sub>O<sub>5</sub> nanowires with an intrinsic peroxidase-like activity. *Adv Funct Mater.* 2011; 21: 501-509.
39. Fan K, Wang H, Xi J, Liu Q, Meng X, Duan D, et al. Optimization of Fe<sub>3</sub>O<sub>4</sub> nanozyme activity via single amino acid modification mimicking an enzyme active site. *Chem Commun (Camb).* 2016; 53: 424-427.
40. Heckman KL, DeCoteau W, Estevez A, Reed KJ, Costanzo W, Sanford D, et al. Custom cerium oxide nanoparticles protect against a free radical mediated autoimmune degenerative disease in the brain. *ACS Nano.* 2013; 7: 10582-10596.
41. Xu C, Qu X. Cerium oxide nanoparticle: A remarkably versatile rare earth nanomaterial for biological applications. *Npg Asia Materials.* 2014; 6: e90.
42. Gupta A, Das S, Neal CJ, Seal S. Controlling the surface chemistry of cerium oxide nanoparticles for biological applications. *Journal of Materials Chemistry B.* 2016; 4: 3195-3202.
43. Fernandez-Garcia S, Jiang L, Tinoco M, Hungria AB, Han J, Blanco G, et al. Enhanced hydroxyl radical scavenging activity by doping lanthanum in ceria nanocubes. *J Phys Chem C.* 2016; 120: 1891-1901.
44. Wang YJ, Dong H, Lyu GM, Zhang HY, Ke J, Kang LQ, et al. Engineering the defect state and reducibility of ceria based nanoparticles for improved anti-oxidation performance. *Nanoscale.* 2015; 7: 13981-13990.
45. Soh M, Kang D-W, Jeong H-G, Kim D, Kim DY, Yang W, et al. Ceria-zirconia nanoparticles as an enhanced multi-antioxidant for sepsis treatment. *Angew Chem Int Ed.* 2017; 56: 11399-11403.
46. Gubernatorova EO, Liu X, Othman A, Muraoka WT, Koroleva EP, Andreescu S, et al. Europium-doped cerium oxide nanoparticles limit reactive oxygen species formation and ameliorate intestinal ischemia-reperfusion injury. *Adv Healthc Mater.* 2017; 6: 1700176.
47. Singh N, Savanur MA, Srivastava S, D'Silva P, Mughes G. A redox modulatory Mn<sub>3</sub>O<sub>4</sub> nanozyme with multi-enzyme activity provides efficient cytoprotection to human cells in a parkinson's disease model. *Angew Chem Int Ed.* 2017; 56: 14267-14271.
48. Song Y, Qu K, Zhao C, Ren J, Qu X. Graphene oxide: Intrinsic peroxidase catalytic activity and its application to glucose detection. *Adv Mater.* 2010; 22: 2206-2210.
49. Montini T, Melchionna M, Monai M, Fornasiero P. Fundamentals and catalytic applications of CeO<sub>2</sub>-based materials. *Chem Rev.* 2016; 116: 5987-6041.
50. Caputo F, Mameli M, Sienkiewicz A, Licocchia S, Stellacci F, Ghibelli L, et al. A novel synthetic approach of cerium oxide nanoparticles with improved biomedical activity. *Sci Rep.* 2017; 7: 4636.
51. Heckert EG, Karakoti AS, Seal S, Self WT. The role of cerium redox state in the SOD mimetic activity of nanoceria. *Biomaterials.* 2008; 29: 2705-2709.
52. Pirmohamed T, Dowding JM, Singh S, Wasserman B, Heckert E, Karakoti AS, et al. Nanoceria exhibit redox state-dependent catalase mimetic activity. *Chem Commun.* 2010; 46: 2736-2738.
53. Naganuma T. Shape design of cerium oxide nanoparticles for enhancement of enzyme mimetic activity in therapeutic applications. *Nano Res.* 2016; 10: 199-217.
54. Li Y, He X, Yin JJ, Ma Y, Zhang P, Li J, et al. Acquired superoxide-scavenging ability of ceria nanoparticles. *Angew Chem Int Ed.* 2015; 54: 1832-1835.
55. Kwon HJ, Cha MY, Kim D, Kim DK, Soh M, Shin K, et al. Mitochondria-targeting ceria nanoparticles as antioxidants for alzheimer's disease. *ACS Nano.* 2016; 10: 2860-2870.
56. Kang D-W, Kim CK, Jeong H-G, Soh M, Kim T, Choi I-Y, et al. Biocompatible custom ceria nanoparticles against reactive oxygen species resolve acute inflammatory reaction after intracerebral hemorrhage. *Nano Res.* 2017; 10: 2743-2760.
57. Bao Q, Hu P, Xu Y, Cheng T, Wei C, Pan L, et al. Simultaneous blood-brain barrier crossing and protection for stroke treatment based on edaravone-loaded ceria nanoparticles. *ACS Nano.* 2018; 12: 6794-6805.
58. Schieber M, Chandel NS. ROS function in redox signaling and oxidative stress. *Curr Biol.* 2014; 24: R453-R462.
59. Patel M. Targeting oxidative stress in central nervous system disorders. *Trends Pharmacol Sci.* 2016; 37: 768-778.
60. Wu H, Li F, Wang S, Lu J, Li J, Du Y, et al. Ceria nanocrystals decorated mesoporous silica nanoparticle based ROS-scavenging tissue adhesive for highly efficient regenerative wound healing. *Biomaterials.* 2018; 151: 66-77.
61. Chigurupati S, Mughal MR, Okun E, Das S, Kumar A, McCaffery M, et al. Effects of cerium oxide nanoparticles on the growth of keratinocytes, fibroblasts and vascular endothelial cells in cutaneous wound healing. *Biomaterials.* 2013; 34: 2194-2201.
62. Chen Z, Wang Z, Ren J, Qu X. Enzyme mimicry for combating bacteria and biofilms. *Acc Chem Res.* 2018; 51: 789-799.
63. Adams C, Bazzigaluppi P, Beckett TL, Bishay J, Weisspapir I, Dorr A, et al. Neuroglial dysfunction in a model of repeated traumatic brain injury. *Theranostics.* 2018; 8: 4824-4836.
64. Xian P, Hei Y, Wang R, Wang T, Yang J, Li J, et al. Mesenchymal stem cell-derived exosomes as a nanotherapeutic agent for amelioration of inflammation-induced astrocyte alterations in mice. *Theranostics.* 2019; 9: 5956-5975.
65. Lee JY, Acosta S, Tuazon JP, Xu K, Nguyen H, Lippert T, et al. Human parthenogenetic neural stem cell grafts promote multiple regenerative processes in a traumatic brain injury model. *Theranostics.* 2019; 9: 1029-1046.
66. Fan K, Xi J, Fan L, Wang P, Zhu C, Tang Y, et al. *In vivo* guiding nitrogen-doped carbon nanozyme for tumor catalytic therapy. *Nat Commun.* 2018; 9: 1440.
67. Yao J, Cheng Y, Zhou M, Zhao S, Lin S, Wang X, et al. ROS scavenging Mn<sub>3</sub>O<sub>4</sub> nanozymes for *in vivo* anti-inflammation. *Chemical science.* 2018; 9: 2927-2933.
68. Liu T, Wang C, Gu X, Gong H, Cheng L, Shi X, et al. Drug delivery with pegylated MoS<sub>2</sub> nano-sheets for combined photothermal and chemotherapy of cancer. *Adv Mater.* 2014; 26: 3433-3440.
69. Mu X, He H, Wang J, Long W, Li Q, Liu H, et al. Carbogenic nanozyme with ultrahigh reactive nitrogen species selectivity for traumatic brain injury. *Nano Lett.* 2019; 19: 4527-4534.
70. Mitchell KJ, Abboud KA, Christou G. Atomically-precise colloidal nanoparticles of cerium dioxide. *Nat Commun.* 2017; 8: 1445.
71. Heckman KL, DeCoteau W, Estevez A, Reed KJ, Costanzo W, Sanford D, et al. Custom cerium oxide nanoparticles protect against a free radical mediated autoimmune degenerative disease in the brain. *ACS Nano.* 2013; 7: 10582-10596.
72. Kim CK, Kim T, Choi IY, Soh M, Kim D, Kim YJ, et al. Ceria nanoparticles that can protect against ischemic stroke. *Angew Chem Int Ed.* 2012; 51: 11039-11043.
73. Lee SS, Song W, Cho M, Puppala HL, Nguyen P, Zhu H, et al. Antioxidant nanoparticles of cerium oxide nanocrystals as a function of nanocrystal diameter and surface coating. *ACS Nano.* 2013; 7: 9693-9703.
74. Tsai Y-Y, Oca-Cossio J, Agering K, Simpson NE, Atkinson MA, Wasserfall CH, et al. Novel synthesis of cerium oxide nanoparticles for free radical scavenging. *Nanomedicine.* 2007; 2: 325-332.
75. Liu H, Hong G, Luo Z, Chen J, Chang J, Gong M, et al. Atomic-precision gold clusters for NIR-II imaging. *Adv Mater.* 2019; 1901015.